Molecular and electronic structure of electroactive self-assembled monolayers

Lucila P. Méndez De Leo, Ezequiel de la Llave, Damián Scherlis, and Federico J. Williams

Citation: J. Chem. Phys. **138**, 114707 (2013); doi: 10.1063/1.4795575
View online: http://dx.doi.org/10.1063/1.4795575
View Table of Contents: http://jcp.aip.org/resource/1/JCPSA6/v138/i11
Published by the American Institute of Physics.

Molecular and electronic structure of electroactive self-assembled monolayers

Lucila P. Méndez De Leo, Ezequiel de la Llave, Damián Scherlis, and Federico J. Williams[a)]

Departamento de Química Inorgánica, Analítica y Química-Física, INQUIMAE-CONICET, Facultad Ciencias Exactas y Naturales, Universidad de Buenos Aires, Pabellón 2, Ciudad Universitaria, Buenos Aires C1428EHA, Argentina

(Received 7 December 2012; accepted 4 March 2013; published online 20 March 2013)

Self-assembled monolayers (SAMs) containing electroactive functional groups are excellent model systems for the formation of electronic devices by self-assembly. In particular ferrocene-terminated alkanethiol SAMs have been extensively studied in the past. However, there are still open questions related with their electronic structure including the influence of the ferrocene group in the SAM-induced work function changes of the underlying metal. We have thus carried out a thorough experimental and theoretical investigation in order to determine the molecular and electronic structure of ferrocene-terminated alkanethiol SAMs on Au surfaces. In agreement with previous studies we found that the Fc-containing alkanethiol molecules adsorb forming a thiolate bond with the Au surface with a molecular geometry 30° tilted with respect to the surface normal. Measured surface coverages indicate the formation of a compact monolayer. We found for the first time that the ferrocene group has little influence on the observed work function decrease which is largely determined by the alkanethiol. Furthermore, the ferrocene moiety lies 14 Å above the metal surface covalently bonded to the alkanethiol SAM and its HOMO is located at −1.6 eV below the Fermi level. Our results provide new valuable insight into the molecular and electronic structure of electroactive SAMs which are of fundamental importance in the field of molecular electronics. © *2013 American Institute of Physics*. [http://dx.doi.org/10.1063/1.4795575]

I. INTRODUCTION

Self-assembled monolayers (SAMs) of alkanethiols on gold provide an important and versatile class of spontaneously organized and structurally well-defined model interfaces. In particular SAMs of electroactive thiols constitute important model systems for the formation of electronic devices by self-assembly.[1] For example, alkanethiol SAMs terminated with Fe^{2+},[2] Ru^{2+},[3] and Os^{2+}[4,5] complexes can serve as good models for studying fundamental phenomena in electron-transfer chemistry. This is due to the fact that the redox groups in the monolayer are at well-defined distances from the underlying metal surface with which they can exchange electrons readily.

Since the pioneering work of Chidsey[2] ferrocene $Fe(C_5H_5)_2$ (Fc) terminated SAMs have been systematically studied. It is well-established that Fc-containing electroactive alkanethiols self-assemble on gold from dilute solutions to form packed monolayers.[1] Furthermore, the electroactive molecules are known to interact with each other perturbing the oxidation-reduction process,[2] which can be avoided by diluting them into an alkanethiol matrix in order to prevent intermolecular interactions between the electroactive moieties. Moreover, immersion of mixed monolayers of alkanethiols and Fc-terminated alkanethiols in solutions of alkanethiols results in the replacement of approximately one-third of the electroactive thiol.[6] The electron-transfer process accompanies a 1:1 ion-pair formation between Fc^+ moieties and anions present in solution.[7] Finally, oxidation of the Fc moieties results in an orientational change which in turn results in a monolayer film thickness increase.[8]

Although these studies have provided significant insight into the structure and electron-transfer processes of Fc-terminated SAMs there are still important issues to be resolved. Particularly, it is important to determine the electronic structure including work function changes induced by the electroactive SAMs. The electronic structure of free ferrocene molecules and related derivatives is very well understood and has been studied over the course of many decades both theoretically and experimentally.[9,10] Furthermore, the electronic structure of adsorbed ferrocene has been studied on Ag(100),[11–13] Cu(100),[11] and Si(111)-(2 × 1).[14] These studies have shown that when the molecule is adsorbed directly on a metal or semiconductor substrate the energies of the molecular orbitals are observed to shift, split, or broaden as a result of the interaction with the underlying surface. There is only one reported investigation on the electronic structure of Fc moieties attached to substrates via a self-assembled monolayer, despite the importance of the system in molecular electronics applications. Johansson and co-workers[15] used a Kelvin probe to determine work function changes induced by the adsorption of ferrocene undecanethiol on Au surfaces. They found that decanethiol SAMs cause a work function decrease whereas ferrocene undecanethiol SAMs cause a very small work function increase.

[a)]Author to whom correspondence should be addressed. Electronic mail: fwilliams@qi.fcen.uba.ar

In this work we study the molecular and electronic structure of self-assembled monolayers of 6-ferrocene 1-hexanethiol (FcC_6), FcC_6 mixed with 1-hexanethiol (C_6), and C_6 over gold using Polarization Modulation Infrared Reflection Absorption Spectroscopy (PM-IRRAS), X-ray and UV photoelectron spectroscopy (XPS and UPS), cyclic voltammetry (CV), and density functional theory calculations (DFT). We found that FcC_6 self-assembles into a compact layer attached via a thiolate bond to the underlying Au surface with the molecules standing upright at approximately 30° with respect to the surface normal. Furthermore, increasing the FcC_6 coverage in the mixed layers results in oxidation/reduction waves broadening and shifting which can be accounted for in terms of the intermolecular interaction of the electroactive centers. UPS measurements identify the HOMO of the Fc moiety located at −1.6 eV with respect to the Au Fermi edge. Moreover, work function changes are mainly determined by the hexanethiol SAM with the non-polar Fc terminal group having no important incidence on its value. These observations are in complete agreement with the results of the theoretical calculations which predict similar trends both in the experimentally measured molecular and electronic structure of the Fc-containing SAMs.

II. EXPERIMENTAL METHODS

Self-assembled monolayer formation, electrochemical, XPS and UPS measurements were performed using an ultra-high vacuum (UHV) chamber equipped with a transfer system built in our laboratory that allows easy and rapid controlled transfer of the sample between the UHV environment and the atmospheric liquid electrochemical environment. The UHV chamber is shown schematically in Figure 1 and is composed of three main subsystems: (i) UHV analysis chamber (2 in Figure 1), (ii) UHV load lock chamber (4 in Figure 1), and (iii) the electrochemical chamber (7 in Figure 1). The UHV chamber is pumped with a turbo molecular pump and a titanium sublimation pump reaching a base pressured $<5 \times 10^{-10}$ mbar. The analysis chamber is equipped with an ion gun for cleaning samples by means of Ar^+ sputtering and with an electron spectrometer system equipped with a 150 mm mean radius hemispherical electron energy analyzer, a nine channeltron detector, a Mg/Al dual X-ray source, and a He I / He II UV radiation source used to carry out XPS and UPS measurements, respectively.

The UHV load lock chamber serves as an intermediate vessel used to insert/remove samples from the laboratory and could be totally isolated from the analysis and electrochemical chambers by means of UHV gate valves (3 and 6 in Figure 1). The electrochemical chamber (7 in Figure 1) is separated from the electrochemical cell (13 in Figure 1) by a gate valve (12 in Figure 1). A sample is transferred from the xyz high precision manipulator in the analysis chamber (1 in Figure 1) to the vertical transfer arm (11 in Figure 1) through the load lock and electrochemical chambers under UHV conditions using two perpendicular horizontal transfer arms (5 and 9 in Figure 1). Once the sample is placed in the vertical transfer arm the electrochemical chamber is pressurized with ultrapure Ar gas prior to opening the gate valve (12 in Figure 1) and translating the sample to the electrochemical cell (13 in Figure 1). The electrochemical cell is a cylindrical Teflon tube with two view ports that allow visual inspection. The cell has the conventional three-electrode configuration that consists of a platinum counter electrode, a Ag/AgCl reference electrode, and the sample as the working electrode. The electrolyte solution employed is filled and drained through a syringe located at the bottom of the cell (17 in Figure 1) into a cell compartment containing both the counter and reference electrodes with a volume of approximately 3 cm^3. The sample position in the vertical direction inside the electrochemical cell could be easily controlled by means of the vertical transfer arm so that a meniscus is formed when contact between the sample and solution is accomplished. The Au crystal employed has a thickness of 5 mm in order to ensure that only its surface is in contact with the electrolyte solution. To minimize contamination of the sample and the electrolyte solution the entire electrochemical chamber and electrochemical cell are pressurized with ultrapure Ar gas. Transferring the sample from the liquid environment of the electrochemical cell to the UHV environment of the analysis chamber implies

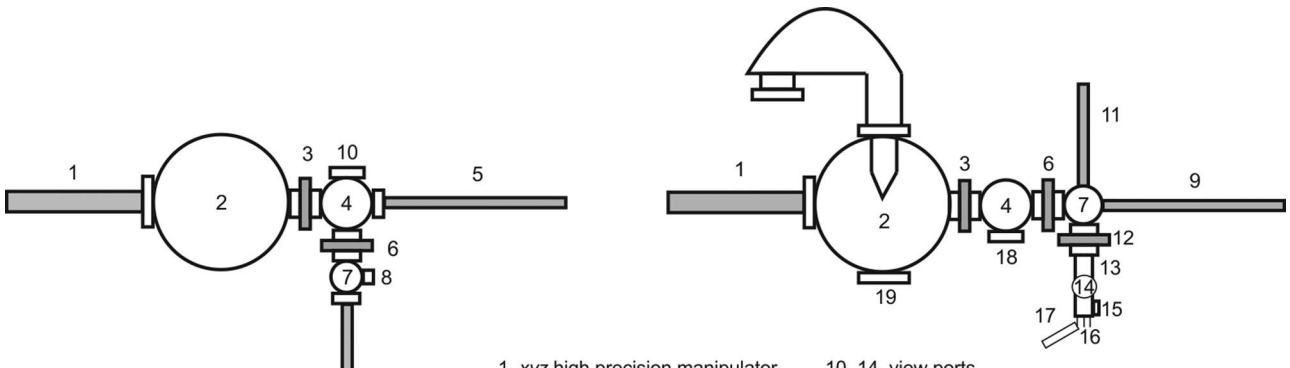

FIG. 1. Schematic of the electrochemical cell–UHV transfer system, (left) top view and (right) side view.

reversing the steps described above evacuating the electrochemical chamber through the load lock chamber.

This transfer system serves the purpose to perform *ex situ* electron spectroscopic measurements on samples that are initially clean in UHV and not exposed to the laboratory atmosphere. Therefore, we have full spectroscopic knowledge of the initial state of the sample before monolayer formation or electrochemical measurements are carried out. Furthermore, the electrochemical cell could be used as both (i) a conventional three-electrode electrochemical cell when controlled by a potentiostat-galvanostat or (ii) a liquid reactor when counter and reference electrodes are not in place and the sample surface is contacted with a well-defined solution forming a meniscus.

A. Monolayer formation

The cylindrical Au crystal with 10 mm diameter and 5 mm thickness is fixed to a Mo sample holder used to manipulate the sample with the different transfer arms. The Au crystal is Ar^+ sputtered (E = 1000 eV) and annealed (T = 670 K) in subsequent cycles until no impurities are detected by XPS (only Au related peaks are observed in the XPS spectra). The spectroscopically clean Au crystal is transferred from the UHV environment to the liquid environment without exposure to the laboratory atmosphere where it forms a meniscus with a previously Ar degassed liquid solution under an Ar atmosphere. Self-assembled monolayers of (i) 6-ferrocene 1-hexanethiol (FcC_6), (ii) a mixture of FcC_6 and 1-hexanethiol (C_6), and (iii) C_6 are formed by contacting the Au crystal with ethanol solutions of (i) 100 μM FcC_6, (ii) 100 μM FcC_6 and 100 μM C_6, and (iii) 100 μM C_6 for 18 h at room temperature. After monolayer formation the solution was removed from the liquid reactor under a constant flow of Ar and the sample was repeatedly rinsed with anhydrous ethanol.

B. Photoelectron spectroscopy

XPS spectra were acquired at a constant pass energy of 20 eV using a MgKα (1253.6 eV) source operated at 12.5 kV and 20 mA and a detection angle of 30° with respect to the sample normal on grounded conducting substrates. Quoted binding energies are referred to the Au $4f_{7/2}$ emission at 84 eV. No charge compensation was necessary and no differential charging features were observed (e.g., low binding energy tails) given that we have measured sufficiently thin films on grounded conducting substrates. Atomic ratios were calculated from the integrated intensities of core levels after instrumental and photoionization cross section corrections. UPS spectra were acquired at a constant pass energy of 2 eV using a He I radiation source (21.2 eV) operated at 1.5 kV and 100 mA with normal detection. Samples were biased at −8 V in order to resolve the secondary electron cutoff in the UPS spectra. Work function values were determined from the width of the UPS spectra as discussed below.

C. IR spectroscopy

PM-IRRAS experiments were performed on a Thermo Nicolet 8700 spectrometer equipped with a custom made external tabletop optical mount, a MCT-A detector (Nicolet), a photoelastic modulator (PEM) (PM-90 with II/Zs50 ZnSe 50 kHz optical head, Hinds Instrument), and Synchronous Sampling Demodulator (SSD) (GWC Instruments). The IR spectra were acquired with the PEM set for a half wave retardation at 1000 cm^{-1} for the low wavenumber region and at 2900 for the high wavenumber region. (We have not measured the region in the 1500 cm^{-1} and 2250 cm^{-1} region as there are no peaks of interest.) The angle of incidence was set at 80°, which gives the maximum of mean square electric field strength for the air/gold interface. The signal was corrected by the PEM response using a method described by Frey *et al.*[16] Typically 1500 scans were performed and the resolution was set for 4 cm^{-1}. Transmission spectrum for FcC_6 was measured using NaCl windows. Resolution was set to 4 cm^{-1} and 200 scans were performed.

D. Electrochemical measurements

Electrochemical measurements were carried out with a potentiostat-galvanostat. All potentials were measured and reported with respect to a Ag/AgCl (3 M KCl) reference electrode. Solutions were prepared using deionized H_2O from a Milli-Q purification system (Millipore Products, Bedford).

E. Materials

6-(Ferrocenyl)hexanethiol (FcC_6) and hexanethiol(C_6) were obtained from Sigma-Aldrich. Absolute ethanol was of analytical grade. XPS and electrochemical experiments were carried out using polycrystalline gold 99.9% purity whereas IR experiments were performed using gold evaporated on glass. These substrates, purchased from Arrandee and consisting of vapor deposited gold films (250 nm in thickness) on a thin layer of chromium supported on glass slides, were flamed annealed in order to generate Au(111) terraces previous monolayer formation.

F. Density functional theory calculations

Electronic structure calculations have been performed using density functional theory[17,18] as implemented in the Quantum Espresso code,[19] which is based on the pseudopotential approximation to represent the ion-electron interactions and plane waves basis sets to expand the Kohn-Sham orbitals. Ultrasoft type pseudo-potentials[20] were adopted, in combination with the PBE formalism to compute the exchange-correlation term.[21] The Au (111) surface was modeled as an infinite bidimensional slab, consisting of four layers of Au atoms truncated at the (111) geometry, and separated from its periodic images in the z direction by a vacuum region of about 12 Å, enough to render the mutual interactions negligible. With the purpose to simulate a surface coverage similar to the one obtained in the experiments, the calculations were performed on supercells of size 5.01 × 5.79 × 32.81 $Å^3$,

containing one adsorbate molecule. In particular, for the computation of the work function, the supercell was expanded to 45.1 Å in the z direction, and molecules were adsorbed on both faces. An energy cutoff of 25 and 200 Ry was used for the plane-waves expansion of the Kohn-Sham orbitals and the charge density, respectively, and a Monkhorst–Pack grid of 5 × 5 × 1 k-points was employed to sample the Brillouin zone. Convergence of the work function and of the density of states was checked against basis set size, k-point sampling, vacuum region, and number of Au layers.

III. RESULTS AND DISCUSSION

A. PM-IRRAS measurements

PM-IRRAS analysis was performed on the modified gold substrates. Figure 1 shows the spectra of Au substrates modified with (a) FcC_6 and (b) a mixture of FcC_6 and C_6. Additionally an IR spectrum of (c) a KBr pellet of FcC_6 was acquired. The bands in the 1200–780 cm^{-1} region correspond to breathing and deformation of the methylenes of the ferrocene ring[22,23] and to CH_2 rocking and C–C stretching of the C_6 alkyl chain.[24] The band at ∼1454 cm^{-1} can be attributed to CH_2 scissoring of the aliphatic tails of the FcC_6 and in spectrum (b) also to C_6,[25–27] while the bands at 1270–1350 cm^{-1} can be ascribed to C–C stretching in the aliphatic chains and in the ferrocene rings.[22,23] It can be easily noted that all of the features of the FcC_6 molecule are observed in all three spectra indicating that the molecules absorb intact on the surface. Furthermore, in PM-IRRAS spectra, the integrated band intensities of absorbed molecules is proportional to $\cos^2\theta$, where θ is the angle between the average direction of the dipole moment and the surface normal.[28] The change in the relative intensity of bands between spectra of the FcC_6 adsorbed on the surface (spectra (a) and (b) in Figure 2) and the spectrum of the KBr pellet of the molecule (spectrum (c) in Figure 2) could be due to preferential orientation of the chains on the gold surface (respect the random orientation of molecules in a KBr pellet). The dipolar moment corresponding to the CH_2 scissoring ($\delta(CH_2)^{C6}$) is perpendicular to the hydrocarbon backbone while that corresponding to the C–C stretching ($\nu(C–C)^{Fc,C6}$) is parallel. The relative increase of the intensity of $\nu(C–C)^{Fc,C6}$ respect to $\delta(CH_2)^{C6}$ indicates that the molecules might be standing up on the surface, with the backbone of the alkyl chains tilted with respect to the surface normal. This observation is consistent with the results of the DFT calculations that predict an angle of approximately 30° with respect to the surface normal. On the high wavenumber region, the peak at ∼3080 cm^{-1} can be attributed to CH stretching of the ferrocene ring, while the peaks at 2928 cm^{-1} and 2855 cm^{-1} are ascribed to the asymmetric and symmetric stretching of CH_2, respectively, in the ferrocene alkyl tails,[25,26] and in the case of the mixture of FcC_6 and C_6 (spectrum (b)) also of C_6. The values where these two peaks appear are consistent with a disordered distribution of the alkyl tails, as expected for this length of chains.[27] Finally, the peak at 2560 cm^{-1} in the free molecule (spectrum (c)) corresponds to the SH stretching.

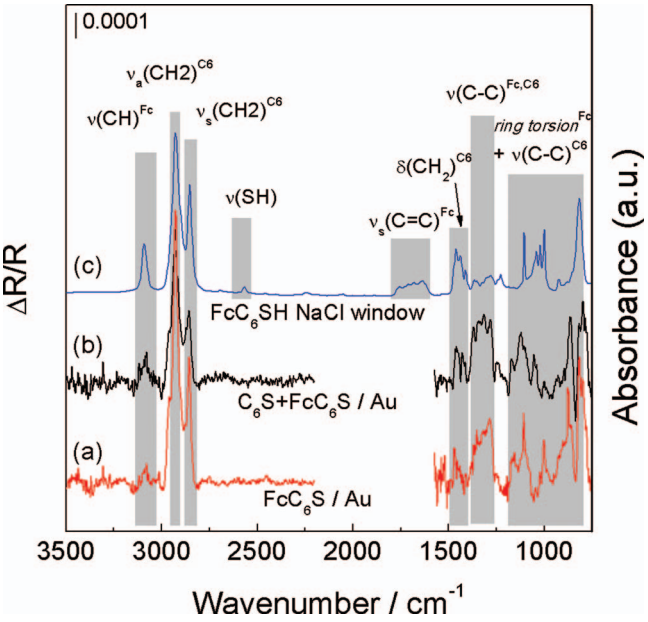

FIG. 2. PM-IRRAS spectra (left axes) corresponding to self-assembled monolayers of (a) ferrocene hexanethiol (FcC_6) and (b) FcC_6 and hexanethiol (FcC_6 + C_6). (c) IR spectrum (right axes) of FcC_6 in a NaCl window.

B. XPS measurements

Self-assembled monolayers of (i) 6-ferrocene 1-hexanethiol (FcC_6), (ii) FcC_6 mixed with 1-hexanethiol (C_6), and (iii) C_6 over Au surfaces were further characterized by XPS. Broad XPS scans show the presence of Fe, C, S, and Au with no other elements being observed in the Au modified surfaces. Figure 3 shows XPS spectra of the (a) Fe 2p, (b) S 2p, (c) C1s, and (d) Au 4f regions corresponding to the (i) bare Au substrate, (ii) FcC_6, (iii) FcC_6 + C_6, and (iv) C_6 modified Au crystal from bottom to top.

The bare Au substrate shows no Fe 2p, S 2p, and C 1s XP signals confirming that the initial condition prior to SAM formation corresponds to a clean Au surface. The C_6 SAM shows no Fe 2p XPS signal as expected whereas the Fe 2p XPS spectra corresponding to the ferrocene containing SAMs (FcC_6 and FcC_6 + C_6) show a Fe $2p_{3/2}$ and Fe $2p_{1/2}$ doublet located at 707.8 eV and 720.7 eV. The position of the doublet is in excellent agreement with previously reported values for adsorbed ferrocene[29] and is consistent with the presence of Fc in its reduced state given that the XPS Fe $2p_{3/2}$ signal of the ferricenium cation is expected at 710.6 eV.[30]

The S 2p XP spectra of all SAMs show a broad signal with a high binding energy shoulder that can be fitted with two sets of doublets each corresponding to the S $2p_{3/2}$ and the S $2p_{1/2}$ components with a spin orbit coupling of 1.2 eV. The low binding energy contribution is centered at 162 eV and corresponds to thiolate bound to the Au surface and it confirms the expected covalent bond formation between the organic thiol and the Au substrate.[31] The high binding energy contribution is centered at 163.5 eV and is attributed to unbound thiol groups which are not covalently bonded to the Au substrate.[31] This later signal corresponds to a 20% (30%) of the total S 2p signal in the cases of the FcC_6 + C_6 and FcC_6 (C_6) monolayers and could be due to FcC_6 or C_6 molecules

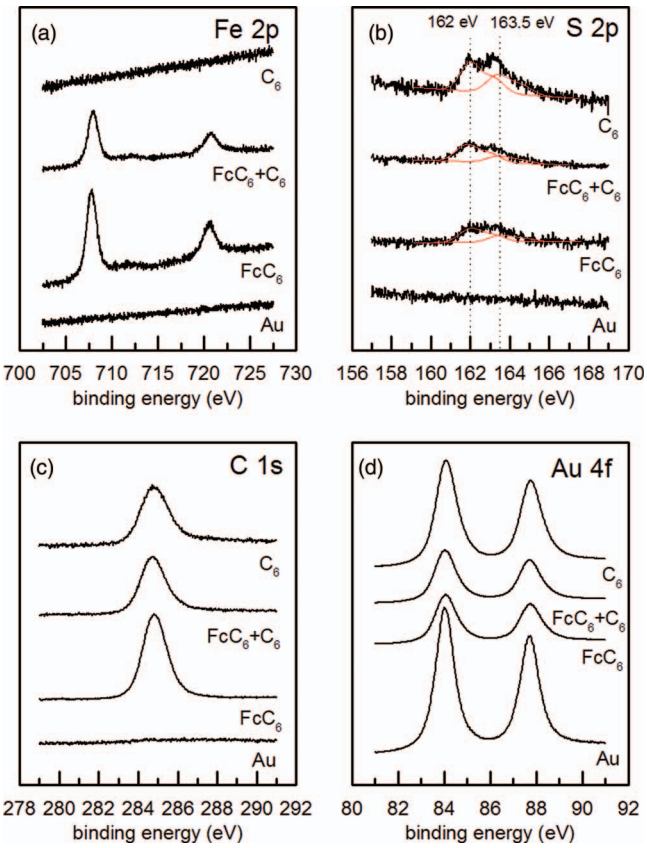

FIG. 3. (a) Fe 2*p*, (b) S 2*p*, (c) C 1*s*, and (d) Au 4*f* XPS spectra corresponding to the bare Au substrate, 6-ferrocene 1-hexanethiol (FcC_6) SAM, mixed SAM of FcC_6 and 1-hexanethiol ($FcC_6 + C_6$), and 1-hexanethiol (C_6) SAM from bottom to top.

that are incorporated into the SAM by lateral interactions with neighboring molecules but without forming a covalent bond with the Au surface.

The C 1*s* spectra corresponding to FcC_6, $FcC_6 + C_6$, and C_6 show one broad signal centered at approximately 284.8 eV which is due to the carbon atoms present in the molecules. The resolution of our measurements did not allow for a clear identification of the carbon atoms in the alkane chain expected at 284.8 eV, the carbon atoms present in the ferrocene ring expected at 284.2 eV, and the carbon atom adjacent to the sulphur endgroup.[15] Clearly the SAM corresponding to FcC_6 has the larger C 1*s* signal as it contains the larger number of C atoms per molecule.

The Au 4*f* spectra corresponding to all cases show the expected Au $4f_{7/2}$ (84 eV) and Au$4f_{5/2}$ (87.7 eV) doublet with a 4:3 intensity ratio. We can estimate the thickness of the SAM from the attenuation of the Au 4*f* XP signal using the following equation:[32] $I = I_0 \exp(-d/\lambda \cos\theta)$, where I (I_0) is the substrate intensity of the SAM covered (bare) surface, d is the SAM thickness, θ is the detection angle with respect to the surface normal, and λ is the photoelectron attenuation length, which for alkanethiols and 1170 eV kinetic energy photoelectrons has a value of approximately 3.4 nm.[33] Formation of the C_6 SAM results in a 82% attenuation of the Au signal ($d/\lambda = 0.197$) from which we can estimate a thickness of ~6.7 Å in excellent agreement with previously reported values.[34] This thickness value results in a tilt angle of the C_6 monolayer of around 30° which is in very good agreement with the DFT calculated value of 30° (see discussion below). The estimated thickness for the FcC_6 SAM is ~24 Å (calculated using the same attenuation length corresponding to alkanethiol SAMs), a greater value than our DFT calculated thickness (see calculations below). This is an overestimation due to the greater electronic density of the ferrocene headgroup which is expected to result in a lower attenuation length for photoelectrons. In fact, the estimated attenuation length of the FcC_6 layer from the DFT calculated thickness is approximately 2 nm. This is the first estimation of the electron attenuation length of ferrocene terminated layers.

The XPS determined C:Fe:S ratio of the FcC_6 SAM is 17.6:1.1:1 in excellent agreement with the stoichiometry of the molecule (16:1:1) and demonstrates that the integrity of the ferrocene thiol molecules is retained after SAM formation. Furthermore, from the integrated Fe 2*p* XPS intensity corresponding to the FcC_6 and $FcC_6 + C_6$ SAMs, we can estimate a surface coverage of 1.8×10^{14} molecules cm^{-2} (FcC_6) and 10^{14} molecules cm^{-2} ($FcC_6 + C_6$). These values suggest that a 1:1 FcC_6:C_6 solution results in a 1:1 FcC_6:C_6 surface coverage suggesting no preferential adsorption as expected given that adsorption is dominated by the S-Au interaction. Furthermore, the XPS estimated surface coverages are in excellent agreement with the values estimated from the electrochemical measurements discussed below.

C. Electrochemical measurements

The FcC_6 SAM and 1:1 FcC_6 monolayer mixed with C_6 ($FcC_6 + C_6$) were transferred from the UHV environment to the liquid environment of the electrochemical cell without exposure to the laboratory atmosphere as described in the experimental section. Figure 4 shows cyclic voltammograms (CV) of Au electrodes modified with FcC_6 (bottom curve) and $FcC_6 + C_6$ (top curve) recorded at a scan rate of 100 mV s^{-1} in the presence of 1 M $NaClO_4$ supporting electrolyte. Oxidation (reduction) waves are observed at 196 mV ($FcC_6 + C_6$) and 383 mV (FcC_6) in line with previously reported values, corresponding to the oxidation (reduction) of the terminal ferrocene group in the monolayer.[35] Here we should point out that lowering the potential further will result in the electroreductive desorption of the hexanethiol molecules. The redox current shows a linear dependence with respect to the scan rates and it is possible to calculate the surface coverage of the electroactive center by integrating the current evolved in a redox cycle. The total charge corresponding to the oxidation of the FcC_6 layer was 26.6 μC and corresponds to a FcC_6 coverage of 2×10^{14} molecules cm^{-2}, whereas in the case of the mixed layer $FcC_6 + C_6$ the total charge was 11.2 μC and corresponds to a FcC_6 coverage of 0.9×10^{14} molecules cm^{-2}. These values are in excellent agreement with the XPS calculated values discussed above and with previously reported values for a full ferrocene layer (2.7×10^{14} cm^{-2}).[2,36] These values are also in agreement with the electrorective desorption measurements of a C_6 SAM. In this case the charge density yields a C_6 surface coverage of 4.6×10^{14} molecules cm^{-2}.

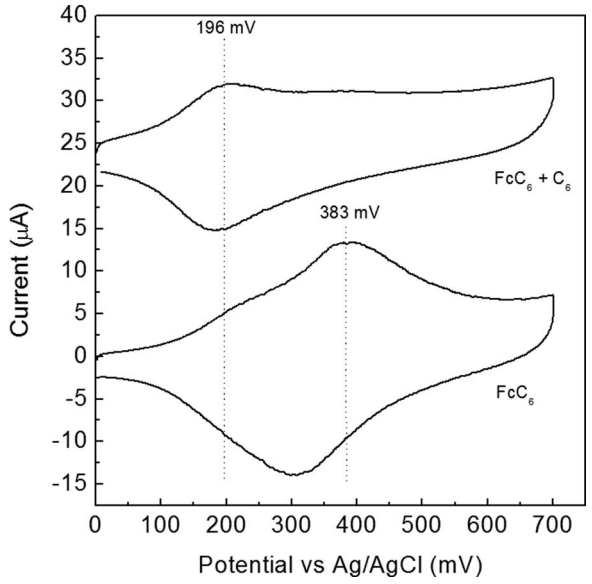

FIG. 4. Cyclic voltammograms of Au electrodes modified with self-assembled monolayers of ferrocene hexanethiol (bottom curve) and a mixed monolayer with hexanethiol (top curve). The voltammograms show a significant change in position and width as the concentration of the electroactive center increases in the monolayer from 10^{14} molecules cm^{-2} ($FcC_6 + C_6$) to 2×10^{14} molecules cm^{-2} (FcC_6). In fact, the $FcC_6 + C_6$ SAM anodic wave has a peak maximum at 196 mV, a full width at half maximum $\Delta E_{FWHM} = 88$ mV and a peak splitting with respect to the cathodic wave $\Delta E = 13$ mV. Whereas in the case of the FcC_6 layer the anodic wave has a maximum at 383 mV, $\Delta E_{FWHM} = 181$ mV, and a peak splitting of 80 mV. These results are in excellent agreement with previously reported studies of ferrocene alkanethiol SAMs[37] and could be accounted for in terms of interacting electroactive species. A positive ferrocenium ion is formed upon oxidation of a ferrocene center and therefore the oxidation of a ferrocene molecule in close proximity will be more difficult as it forms another positive charge and it therefore requires a more anodic potential. Thus the anodic peak is expected to shift to greater values as the FcC_6 coverage in the SAM increases. Furthermore, the full width at half maximum of the anodic wave provides an indication of the interactions taking place between different centers[37] therefore explaining the observed increase in ΔE_{FWHM} with increasing FcC_6 coverage in the SAM. Finally, at low ferrocene coverage a 13 mV peak splitting between the anodic and cathodic sweep can be observed as a result of the fast enough electron-transfer kinetic, while an increase of the electroactive molecule in the layer leads to a peak splitting of 80 mV.

The surface coverage of C_6 is larger than that of FcC_6 given the bulky nature of the Fc group absent in the first case. We should finally note that the surface coverage of the FcC_6 molecule varies with the FcC_6 to C_6 ratio in the ethanolic preparing solution.[36]

D. UPS measurements

Figure 5 shows the UP spectra of FcC_6, C_6, and $FcC_6 + C_6$ monolayers on Au surfaces in comparison to the spectrum of the clean gold surface. The left panel shows the secondary electron cutoff and the right panel shows the region around the Fermi edge. The UPS spectrum corresponding to the bare Au substrate shows the same pattern and peak positions (2.7 and 4.3 eV vs EF) to that previously reported for clean Au surfaces and corresponds to the 5*d* bands.[38] At this point it is important to note that the escape depth (or attenuation length) λ of photoelectrons with 15 eV kinetic energy,

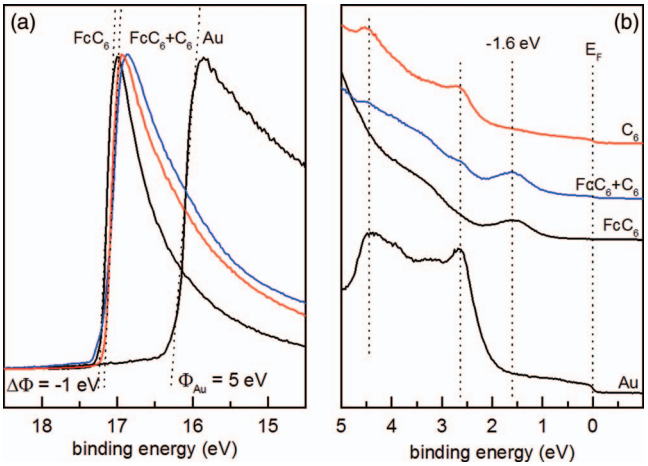

FIG. 5. UPS spectra of the bare gold substrate (Au), SAM of ferrocene hexanethiol (FcC_6), mixed SAM with hexanethiol ($FcC_6 + C_6$), and hexanethiol (C_6, red curve) showing (a) work function changes ($\Delta\Phi$) calculated from the secondary electron cutoff and (b) density of states below the Fermi level.

i.e., below the Fermi edge photoemission for Au in a He(I) experiment, is approximately 8 Å for a compact hydrocarbon film.[39] Therefore, the sampling depth in the photoemission experiment at zero degrees take-off angle is approximately 24 Å (3 λ) hence this experiment samples the entire SAM layer and the SAM/Au interface.

From the width (W) of the UPS spectrum we can calculate the work function (Φ)[40] of our Au substrates: $\Phi = 21.2$ eV $-$ W $= 5$ eV which is in excellent agreement with values reported for polycrystalline gold.[35] Work functions (Φ) are comprised of a surface potential (χ) due to dipoles present on the surface and to the chemical potential of the electron in the metal (μ) due to the interaction of the electron with the bulk of the metal, $\Phi = \chi - \mu/e$.[41] Therefore, changes in metal work functions could be due to changes in the bulk properties of the metal or in the surface potential by modifying the dipole of the surface layer. Chemisorbed alkanethiols form a dipole layer with negative charges residing at the metal/monolayer interface and positive charges at the monolayer/vacuum interface, thus alkanethiol monolayers chemisorbed on metal surfaces cause a work function decrease on Au[42], Ag,[43] and Cu.[44] Furthermore, replacing the $-CH_3$ end group in the alkanethiol SAM by electronegative chemical groups reverses the direction of the dipole and causes a work function increase.[45,46] Thus the metal work function can be tuned over a wide range (-2 eV to 2 eV) depending on the functional group at the end of the thiol molecule forming the SAM.[47]

Figure 5 shows that when the FcC_6, C_6, or $FcC_6 + C_6$ monolayer is adsorbed on the metal surface the Au 5*d* bands decrease in intensity indicating the presence of the adsorbate[39] and shifting the position of the secondary electron cutoff which indicates a decrease in the Au work function. Formation of FcC_6, C_6, and $FcC_6 + C_6$ monolayers over Au surfaces results in a work function change of approximately -1 eV in all cases (within the experimental uncertainty of 500 meV). Alkanethiol SAMs with 3–18 carbon atoms are known to change the work function of Au by -1 to

−1.2 eV[48,49] in line with our measured value for hexanothiol. Incorporation of ferrocene at the end of the hexanothiol chain is not expected to modify the work function as the electroactive molecule has no net dipole and should not modify the surface dipole layer, hence we observe a similar value for the work function change of the FcC_6, C_6, and $FcC_6 + C_6$ monolayers $\Delta\Phi \approx -1$ eV. Here we should note that this result is at variance with recently published studies of the interaction of a 11-ferrocene 1-undecanethiol (FcC_{11}) SAM over Au surfaces where the FcC_{11} induced work function change was $\Delta\Phi = +0.036$ eV.[15] The authors used a Kelvin probe operated in ambient air conditions in order to determine the work function changes induced by the FcC_{11} SAM. Therefore, differences in work function changes could be due to surface impurities which have a profound effect in the work function and are minimized in our case as experiments are carried out in clearly defined conditions.

The hexanethiol SAM is expected to have photoemission lines in the 7–10 eV range of the He(I) UPS spectrum superimposing with the Au 5*d* signals with the HOMO level located above 6 eV.[39] Therefore, we did not observe any distinguishable new feature in the UPS spectrum of C_6. However, UPS spectra of FcC_6 and $FcC_6 + C_6$ show a clear band located at −1.6 eV with respect to the Fermi edge. The first photoemission band in the UPS spectrum corresponding to ferrocene in the gas phase is located at 6.7 eV (e_{2g}).[9] This band would appear at approximately −1.7 eV with respect to the Fermi edge subtracting the Au work function of 5 eV since the original energy scale of the UPS gas-phase spectrum is relative to the vacuum level. All other FcC_6 photoemission bands due to the ferrocene group will be superimposed with the Au 5*d* bands and hence not discernable in the measured spectra. Therefore, we can assign the observed band at −1.6 eV with photoemission from the HOMO e_{2g} molecular orbital (with ring orbital and Fe $3d_{xy}$ and $3d_{x^2-y^2}$ components) of ferrocene in the self-assembled monolayer. This assignment is further explored in the DFT calculations discussed below. We should note that adsorbed ferrocene molecules on Ag(100)[12] and Cu(100)[11] have photoemission bands from the e_{2g} molecular orbital at −4.6 eV and −4.2 eV below the Fermi edge, respectively. In those studies the ferrocene molecule interacts directly with the metal surface modifying the relative energies of the molecular orbitals, whereas in the present study the ferrocene group lies 12 Å away from the Au surface so that a direct comparison (corrected by the work function) with the gas phase spectrum is possible.

The HOMO energy of an adsorbed redox probe as determined by UPS is related with its oxidation potential as determined by CV via the following experimental equation: E_{HOMO} (vs VL) $= -1.4 \times qV_{CV}$ (vs Fc) − 4.6 eV.[50] We can therefore calculate the position of the HOMO relative to the vacuum level using the measured oxidation potential (Figure 4). The oxidation potential of "isolated" Fc is V_{CV} (vs Fc) = 0.196 V + 0.45 V = 0.646 V which results in E_{HOMO} (vs VL) = 5.5 eV. Given that the Φ of the FcC_6 modified Au surface is 4 eV the HOMO position with respect to the Fermi level should be −1.5 eV which provides additional evidence that the UPS band located at approximately −1.6 eV corresponds to photoemission from the FcC_6 HOMO.

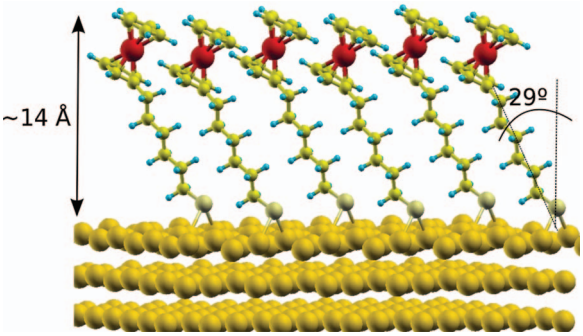

FIG. 6. Structure of the FcC_6 monolayer on the Au surface, as obtained from a DFT relaxation in periodic boundary conditions. For image clarity, the depicted surface coverage is only one fourth of the actual coverage used in the simulations. Labels in black indicate the optimized width of the monolayer and angle of the hydrocarbon chains with respect to the surface normal.

E. DFT calculations

Figure 6 presents the optimized FcC_6 complex on the Au (111) slab. For clarity, the number of FcC_6 molecules per unit area represented in the figure is $\frac{1}{4}$ of the one used in our calculations: our periodic model contained an adsorbate molecule per supercell, which corresponds to a surface coverage of 3.4×10^{14} molecules cm^{-2}. Optimization of this model system was performed relaxing all atoms, with the exception of the inner two layers of the metallic slab, which were frozen to reproduce the positions of the bulk metal. For this coverage, we found the alkyl chains subtend an angle of 29° with respect to the surface normal, similarly to what has been reported experimentally and computationally for the tilt of alkanethiols of this length on gold.[51] On the other hand, the cyclopentadienyl rings of the ferrocene moiety are staggered (rotated 180° with respect to each other), as has been reported in the solid state,[52] and form an angle of 18° with the Au surface, implying a tilt of 72° with respect to the surface normal. In Ref. 15, Johansson *et al.* report values ranging from 27° to 36° for this tilt in mixed FcC_{11}/C_{10} monolayers, depending on the fraction of decanethiol in the SAM. This means that, according to their measurements, the orientation of the ring is less parallel to the interface than in our DFT simulations. A likely reason for this discrepancy is the difference in surface coverages: we recall that in our DFT model the FcC_6 concentration is around 70% above the experiment. In such a dense monolayer, the bulky Fc groups would tend to minimize the repulsive interactions, and one way to achieve this is by lying parallel to the surface. The FcC_{11} coverage is not reported in Ref. 15, but, based on the preparation procedures, it is presumably not too different from the one in our experiments, and therefore lower than in the calculations. Possibly for the same reason, the inclination reported in Ref. 15 for the hydrocarbon chain is moderately larger than in our simulations (46° versus 29°). The total thickness of the SAM resulting from the structure relaxation is nearly 14 Å: this value has been adopted to estimate the photoelectron attenuation length λ discussed above.

DFT has proved to be a reliable tool to compute work functions of clean and functionalized metal surfaces, in

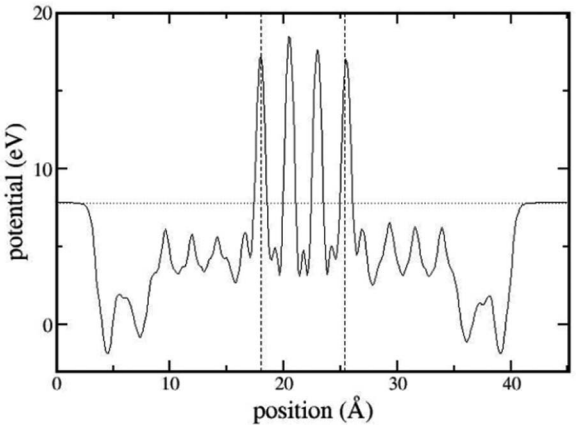

FIG. 7. Electrostatic potential as a function of the z position (normal to the surface), calculated from DFT for the FcC_6/Au(slab)/FcC_6 model. The values are averaged on the x, y plane at every point along the z direction. The dashed vertical lines indicate the boundaries of the slab (or the z-coordinates of the Au atoms of the external layers), and the dotted horizontal line marks the vacuum level, equal to 7.84 eV. The work function is calculated from the difference between the vacuum and the Fermi energies, 7.84–3.58 eV = 4.26 eV.

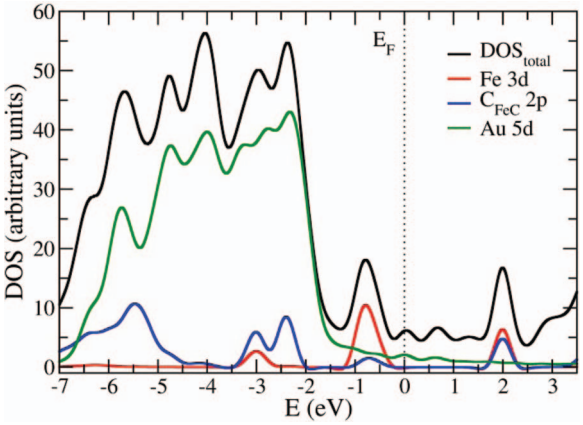

FIG. 8. Total and projected density of states around the Fermi level, computed with DFT for the system comprising the FcC_6 adsorbate plus the Au slab.

particular for alkyl-thiols on gold.[46,53,54] The work function Φ is calculated from the energy difference between the electrostatic potential in the vacuum region, and the Fermi level. To this end, the supercell must be large enough in the direction perpendicular to the surface, to allow for the electrostatic potential to reach a plateau far away from the interface, in the vacuum region. For the clean Au (111) surface, we obtained $\Phi = 5.34$ eV, slightly above the value estimated for our polycrystalline sample via XPS and UPS, but in excellent accord with previous photoemission experiments on the (111) face of gold.[53,55] For the computation of Φ in the presence of the SAM, simulations were performed with both exposed faces covered with the adsorbate, with a supercell expanded to 45.1 Å in the z-direction. Figure 7 shows the variation of the (averaged) electrostatic potential along the direction normal to the surface for the FcC_6 system: the potential reaches a constant value at nearly 17 Å away from the Au/FcC_6 interface, which was used to calculate Φ. This procedure provides estimates of 4.19 eV and 4.26 eV for the work functions of the C_6 and the FcC_6 systems, respectively, therefore the shifts with respect to the clean surface turn out to be −1.15 eV and −1.08 eV. These results are in very good agreement with the shifts obtained from our UPS data, supporting the notion that the presence of the ferrocene group has not a major effect on the work function. The marginally larger shifts found in the calculations, by about 0.1 eV, may be related to the fact that the surface coverage modeled with DFT was higher than in the experimental sample.

Figure 8 depicts the total and projected density of states for the FcC_6 system. Among the main features, it can be seen the broad signal corresponding to the 5d states shows a first maximum at −2.4 eV, with the highest peak at −4.0 eV. These features are in general agreement with the UPS spectra of the clean surface presented in Figure 5. In the same figure, the Au 5d signals for the C_6 and FcC_6 systems appear significantly attenuated and partially distorted, due to the physical barrier imposed by the organic layer. This effect is of course not present in our simulated spectra, and therefore the computed positions of the 5d states in the case of the clean surface (not shown) do not differ from those obtained for the FcC_6 model in Figure 8, which in time resemble the experimental data for the bare substrate. In comparison with the measured data, the DFT calculated signals are slightly more positive. However, we recall the experimental density of states of gold may show a variability of some tenths of eV, because the exact positions of the bands depend on the exposed Au crystallographic face and are affected by the energy of the incident photons, the detection angle, and other details of the experimental setup.[56,57] The projected density of states reveal that the first peak arising below the Fermi edge, centered at around −0.8 eV, is originating in the d electrons of the ferrocene iron. The position of this band is shifted nearly 0.8 eV with respect to the UPS spectra of Figure 5. The reason behind this discrepancy is not evident to us, but it may be partially attributed to the difference between the calculated and measured work functions, which accounts already for a positive shift of 0.3 eV, and to a possible disorder in the FcC_6 moieties, which could be responsible for the broadening of the experimental band. The difference in surface coverages between the model and the sample might also be contributing to this disagreement. Projection of the density of states into the different d components shows that this peak has major contributions from the $d_{x^2-y^2}$, d_{xy}, and d_{z^2} orbitals of the Fe atom. This band can be identified with the HOMO (e_{2g}) of the ferrocene molecule, which has been described in terms of the same d orbitals via electronic structure calculations in the gas phase.[58] The relative intensities of the Au 5d and Fe 3d signals is simply reflecting the ratio between the number of d electrons in the adsorbate and in the slab.

IV. CONCLUSIONS

We have investigated the molecular and electronic structure of pure FcC_6 and FcC_6 mixed with C_6 self-assembled monolayers over Au surfaces using a broad range of spectroscopic techniques as well as density functional theory calculations. SAMs were prepared using a liquid reactor attached to

an UHV analysis chamber. Our experimental setup allows carrying out experiments using spectroscopically well-defined substrates without exposing the clean or the SAM functionalized crystals to the laboratory atmosphere. Experimental measurements indicate that the electroactive molecules self-assemble into a compact monolayer forming a thiolate bond with the underlying Au surface. The molecules in the monolayer are standing upright forming an angle of approximately 30° with respect to the surface normal. Furthermore, the electroactive group retains its molecular integrity upon formation of the monolayer. Unlike electronic structure studies of Fc molecules adsorbed on metal surfaces which indicate that the Fc HOMO orbital interacts strongly with the metal electrons, our UPS measurements and DFT calculations indicate that the Fc molecule retains its electronic structure as the ferrocene group lies 12 Å away from the Au surface. Moreover, we have identified the Fc HOMO orbital as the e_{2g} orbital located at approximately −1.6 eV below the Fermi level. Finally we have observed that SAMs of Fc containing alkanethiols results in a work function decrease of the Au substrate demonstrating that the work function of Fc containing SAMs is largely determined by the alkanethiol molecule with a negligible contribution from the nonpolar electroactive moiety.

ACKNOWLEDGMENTS

Funding from CONICET, UBA, and AGENCIA is gratefully acknowledged. We acknowledge time allocation for all the DFT calculations in the supercomputer *Cristina* funded by ANPCYT.

[1] C. E. D. Chidsey, Science **251**, 919 (1991).
[2] C. E. D. Chidsey, C. R. Bertozzi, T. M. Putvinski, and A. M. Mujsce, J. Am. Chem. Soc. **112**, 4301 (1990).
[3] H. O. Finklea and D. D. Hanshew, J. Am. Chem. Soc. **114**, 3173 (1992).
[4] A. M. Ricci, N. Tognalli, E. de la Llave, C. Vericat, L. P. Mendez De Leo, F. J. Williams, D. Scherlis, R. Salvarezza, and E. J. Calvo, Phys. Chem. Chem. Phys. **13**, 5336 (2011).
[5] P. Salvatore, A. Glargaard Hansen, K. Moth-Poulsen, T. Bjornholm, R. John Nichols, and J. Ulstrup, Phys. Chem. Chem. Phys. **13**, 14394 (2011).
[6] D. M. Collard and M. A. Fox, Langmuir **7**, 1192 (1991).
[7] Y. Yokota, T. Yamada, and M. Kawai, J. Phys. Chem. C **115**, 6775 (2011).
[8] S. Ye, Y. Sato, and K. Uosaki, Langmuir **13**, 3157 (1997).
[9] J. W. Rabalais, L. O. Werme, T. Bergmark, L. Karlsson, M. Hussain, and K. Siegbahn, J. Chem. Phys. **57**, 1185 (1972).
[10] A. Boccia, A. G. Marrani, S. Stranges, R. Zanoni, M. Alagia, M. Cossi, and M. F. Iozzi, J. Chem. Phys. **128**, 154315 (2008).
[11] C. Waldfried, D. Welipitiya, C. W. Hutchings, H. S. V. de Silva, G. A. Gallup, P. A. Dowben, W. W. Pai, J. Zhang, J. F. Wendelken, and N. M. Boag, J. Phys. Chem. B **101**, 9782 (1997).
[12] D. Welipitiya, P. A. Dowben, J. Zhang, W. W. Pai, and J. F. Wendelken, Surf. Sci. **367**, 20 (1996).
[13] D. Welipitiya, A. Green, J. P. Woods, P. A. Dowben, B. W. Robertson, D. Byun, and J. Zhang, J. Appl. Phys. **79**, 8730 (1996).
[14] R. Zanoni, M. N. Piancastelli, M. Marsi, and G. Margaritondo, J. Electron Spectrosc. Relat. Phenom. **57**, 199 (1991).
[15] S. Watcharinyanon, E. Moons, and L. S. O. Johansson, J. Phys. Chem. C **113**, 1972 (2009).
[16] *Polarization-modulation Approaches to Reflection-Absorption Spectroscopy*, edited by B. L. Frey, R. M. Corn, and S. C. Weibel (John Wiley & Sons, 2001), Vol. 2.
[17] P. Hohenberg and W. Kohn, Phys. Rev. **136**, B864 (1964).
[18] W. Kohn and L. J. Sham, Phys. Rev. **140**, A1133 (1965).
[19] P. Giannozzi, S. Baroni, N. Bonini, M. Calandra, R. Car, C. Cavazzoni, D. Ceresoli, G. L. Chiarotti, M. Cococcioni, I. Dabo, A. Dal Corso, S. de Gironcoli, S. Fabris, G. Fratesi, R. Gebauer, U. Gerstmann, C. Gougoussis, A. Kokalj, M. Lazzeri, L. Martin-Samos, N. Marzari, F. Mauri, R. Mazzarello, S. Paolini, A. Pasquarello, L. Paulatto, C. Sbraccia, S. Scandolo, G. Sclauzero, A. P. Seitsonen, A. Smogunov, P. Umari, and R. M. Wentzcovitch, J. Phys.: Condens. Matter **21**, 395502 (2009).
[20] D. Vanderbilt, Phys. Rev. B **41**, 7892 (1990).
[21] J. P. Perdew, K. Burke, and M. Ernzerhof, Phys. Rev. Lett. **77**, 3865 (1996).
[22] T. P. Gryaznova, S. A. Katsyuba, V. A. Milyukov, and O. G. Sinyashin, J. Organomet. Chem. **695**, 2586 (2010).
[23] N. Mohammadi, A. Ganesan, C. T. Chantler, and F. Wang, J. Organomet. Chem. **713**, 51 (2012).
[24] N. Sandhyarani and T. Pradeep, Vacuum **49**, 279 (1998).
[25] L. J. Bellamy, *The Infra-red Spectra of Complex Molecules*, 2nd ed. (Methuen & Co Ltd., London, 1958).
[26] D. Lin-Vein, N. B. Colthup, W. G. Fateley, and J. G. Grasselli, *The Handbook of Infrared and Raman Characteristic Frequencies of Organic Molecules* (Academic Press, Inc., San Diego, CA, 1991).
[27] M. D. Porter, T. B. Bright, D. L. Allara, and C. E. D. Chidsey, J. Am. Chem. Soc. **109**, 3559 (1987).
[28] V. Zamlynny and J. Lipkowski, in *Advances in Electrochemical Science and Engineering*, edited by R. C. Alkire, D. M. Kolb, J. Lipkowski, and P. N. Ross (Wiley, Weinheim, 2006), Vol. 9.
[29] C. M. Woodbridge, D. L. Pugmire, R. C. Johnson, N. M. Boag, and M. A. Langell, J. Phys. Chem. B **104**, 3085 (2000).
[30] M. Umaña, D. R. Rolison, R. Nowak, P. Daum, and R. W. Murray, Surf. Sci. **101**, 295 (1980).
[31] M.-C. Bourg, A. Badia, and R. B. Lennox, J. Phys. Chem. B **104**, 6562 (2000).
[32] P. E. Laibinis, C. D. Bain, and G. M. Whitesides, J. Phys. Chem. **95**, 7017 (1991).
[33] C. D. Bain and G. M. Whitesides, J. Phys. Chem. **93**, 1670 (1989).
[34] H. A. Biebuyck, C. D. Bain, and G. M. Whitesides, Langmuir **10**, 1825 (1994).
[35] K. Uosaki, Y. Sato, and H. Kita, Langmuir **7**, 1510 (1991).
[36] G. K. Rowe and S. E. Creager, Langmuir **7**, 2307 (1991).
[37] T. Auletta and F. C. J. M. van Veggel, and D. N. Reinhoudt, Langmuir **18**, 1288 (2002).
[38] L. Scudiero, D. E. Barlow, U. Mazur, and K. W. Hipps, J. Am. Chem. Soc. **123**, 4073 (2001).
[39] A. S. Duwez, G. Pfister-Guillouzo, J. Delhalle, and J. Riga, J. Phys. Chem. B **104**, 9029 (2000).
[40] D. Cahen and A. Kahn, Adv. Mater. **15**, 271 (2003).
[41] H. Reiss, J. Phys. Chem. **89**, 3783 (1985).
[42] S. D. Evans and A. Ulman, Chem. Phys. Lett. **170**, 462 (1990).
[43] I. H. Campbell, S. Rubin, T. A. Zawodzinski, J. D. Kress, R. L. Martin, D. L. Smith, N. N. Barashkov, and J. P. Ferraris, Phys. Rev. B **54**, R14321 (1996).
[44] I. H. Campbell, J. D. Kress, R. L. Martin, D. L. Smith, N. N. Barashkov, and J. P. Ferraris, Appl. Phys. Lett. **71**, 3528 (1997).
[45] S.-H. Lee, W.-C. Lin, C.-J. Chang, C.-C. Huang, C.-P. Liu, C.-H. Kuo, H.-Y. Chang, Y.-W. You, W.-L. Kao, G.-J. Yen, D.-Y. Kuo, Y.-T. Kuo, M.-H. Tsai, and J.-J. Shyue, Phys. Chem. Chem. Phys. **13**, 4335 (2011).
[46] P. C. Rusu and G. Brocks, J. Phys. Chem. B **110**, 22628 (2006).
[47] G. Heimel, L. Romaner, J.-L. Brédas, and E. Zojer, Phys. Rev. Lett. **96**, 196806 (2006).
[48] D. M. Alloway, M. Hofmann, D. L. Smith, N. E. Gruhn, A. L. Graham, R. Colorado, V. H. Wysocki, T. R. Lee, P. A. Lee, and N. R. Armstrong, J. Phys. Chem. B **107**, 11690 (2003).
[49] D. Fragouli, T. N. Kitsopoulos, L. Chiodo, F. Della Sala, R. Cingolani, S. G. Ray, and R. Naaman, Langmuir **23**, 6156 (2007).
[50] B. W. D'Andrade, S. Datta, S. R. Forrest, P. Djurovich, E. Polikarpov, and M. E. Thompson, Org. Electron. **6**, 11 (2005).
[51] C. Vericat, M. E. Vela, G. A. Benitez, J. A. M. Gago, X. Torrelles, and R. C. Salvarezza, J. Phys.: Condens. Matter **18**, R867 (2006).
[52] J. D. Dunitz and L. E. Orgel, Nature (London) **171**, 121 (1953).
[53] V. De Renzi, R. Rousseau, D. Marchetto, R. Biagi, S. Scandolo, and U. del Pennino, Phys. Rev. Lett. **95**, 046804 (2005).
[54] A. Nagoya and Y. Morikawa, J. Phys.: Condens. Matter **19**, 365245 (2007).
[55] G. V. Hansson and S. A. Flodström, Phys. Rev. B **18**, 1572 (1978).
[56] R. J. Baird, L. F. Wagner, and C. S. Fadley, Phys. Rev. Lett. **37**, 111 (1976).
[57] P. H. Citrin, G. K. Wertheim, and Y. Baer, Phys. Rev. Lett. **41**, 1425 (1978).
[58] Z.-F. Xu, Y. Xie, W.-L. Feng, and H. F. Schaefer, J. Phys. Chem. A **107**, 2716 (2003).